Applications of electron channeling pattern for the determination of wafer offcut and misorientation angles

Han, Han; Strakos, Libor; Porret, Clement; DEPAUW, Valerie; Vystave, Tomas; Richard, Olivier; Baryshnikova, Marina; Grieten, Eva & Hantschel, Thomas (2025)
Applications of electron channeling pattern for the determination of wafer offcut and misorientation angles. In: Micron, 199 (Art N° 103912).

DOI: 10.1016/j.micron.2025.103912
Handle: http://hdl.handle.net/1942/47568

Applications of electron channeling pattern for the determination of wafer offcut and misorientation angles

Han Han[a*], Libor Strakos[b], Clément Porret[a], Valérie Depauw[a,c,d], Tomas Vystavel[b], Olivier Richard[a], Marina Baryshnikova[a], Eva Grieten[a], and Thomas Hantschel[a]

[a] imec, Kapeldreef 75, 3001 Leuven, Belgium

[b] Thermo Fisher Scientific, Vlastimila Pecha 12, 62700 Brno, Czech Republic

[c] Hasselt University, imo-imomec, Martelarenlaan 42, 3500 Hasselt, Belgium

[d] EnergyVille, imo-imomec, Thor Park 8320, 3600 Genk, Belgium

[*]Han.Han@imec.be

Abstract

The epitaxial growth of semiconductor multilayers often starts from monocrystalline wafers that have an offcut angle. This offcut angle is critical for tailoring the properties of epitaxial materials, making its precise control essential. This study demonstrates a novel approach to determine the wafer offcut angle based on electron channeling patterns (ECP) obtained by scanning electron microscopy. The technique involves calculating the angular distance between the zone axis and the surface normal by analyzing a series of ECP images acquired at various rotations/tilts. The method successfully applies to Si(001) substrates with different offcut angles, measured within ~ 1 hour with an angular accuracy of ~ 0.05°. Additionally, the misorientation between the overlaying semiconductor crystalline films and the substrate is estimated with a precision down to ~ 0.03º within ~ 30 minutes. This performance can meet the accuracy requirements for a wide range of industrial and research applications.

Keywords

Wafer offcut angle, misorientation, electron channeling pattern

1. Introduction

Advanced semiconductor devices used in various fields such as electronics, opto-electronics, photonics and power electronics are frequently based on epitaxial layers grown on silicon or III-V wafers. Material properties, including strain and crystalline defect, play a critical role in device characteristics and performances. These properties can typically be optimized by selecting substrates with proper wafer offcut angles. In general, the wafer offcut angle is termed as the angle between the wafer surface normal and the closest low-index zone axis, referred to as zone axis in this article. The Si substrate has a 0° offcut angle, if the Si ingot is cut perpendicularly to the [001] or other zone axis. Otherwise, the offcut angle is non 0°. The significance of choosing a wafer with a suitable offcut angle has already been demonstrated for different material systems. For example, a 4° offcut angle has proven beneficial to the

heterogeneous integration of high quality III-V on Si(001) wafers to reduce the density of anti-phase boundaries (APB) [1-3]. For the epitaxial growth of GaN material systems, the wafer offcut angle can influence not only the surface morphology [4,5], but also the incorporation rate of indium into the epitaxial layer [4,6]. Furthermore, the density of twins generated during the homoepitaxial growth on (100) β-Ga_2O_3 significantly depends on the wafer offcut angle and a defect-free epi-layer can be achieved thanks to a 6° wafer offcut angle [7]. For wafer-scale epitaxial growth of two-dimensional (2D) materials, the homogeneity and conductivity of 2D layers can be significantly improved by using sapphire wafers with a 1° offcut angle [8]. The selection of the correct wafer offcut angle is therefore crucial to the semiconductor device performance. However, the offcut angle of such wafer substrates is usually provided with a certain tolerance, which may not guarantee sufficient process control. Therefore, the wafer offcut angle must in some cases be accurately determined before the epitaxial growth. After epitaxial growth, the misorientation of the epitaxial layers with respect to the vicinal substrate is frequently observed in many material systems due to relaxation processes [9,10]. Such misorientations can reach several degrees, thus impacting critical material properties such as mechanical stability and electrical conductivity. Therefore, it is also of crucial importance to measure and monitor any changes in the orientation of such epitaxial layers.

To characterize the wafer offcut angle and the misorientation between the overlaying crystalline layer and the substrate, high resolution X-ray diffraction (HRXRD) is considered as a standard technique, offering an absolute angular resolution of ~ 0.01° [11,12]. Alternatively, electron backscatter diffraction (EBSD) can measure the relative misorientation, achieving an angular resolution of approximately 0.1° [13]. Such angular resolution can further be improved at the expense of complicated post data analysis [14]. However, the absolute angular resolution with respect to the microscope's optical axis can be up to ~ 1° to 2° due to the 70° tilting geometry [15]. While these techniques are commonly used, they are often time-consuming and involve complex analyses. Furthermore, HRXRD measurements can be significantly time-consuming for high offcut angles. Relatively fast measurements are preferred, however, at the expense of angular resolution. As a result, other techniques are needed for rapid and accurate measurements of the wafer offcut and misorientation for both engineers and researchers in the semiconductor fields. In this study, we propose a novel approach based on electron channeling patterns (ECP) obtained by scanning electron microscopy (SEM).

In SEM, Kikuchi-like ECPs can be observed, superimposed on backscattered electron (BSE) images of bulk single crystals. During SEM imaging at low magnifications, the electron beam incident angle varies as the electron probe scans the sample. As a result, the electron can channel down at Bragg angles for certain sets of lattice planes, leading to a decrease of the BSE intensity. This generates a set of electron channeling bands (ECB) appearing as dark lines, which further form the so-called ECP on BSE images. ECPs can therefore be indexed according to the sample crystallographic orientations. ECPs

were first theoretically predicted by Hirsch [16] in 1962, afterwards experimentally observed by Coates [17] and interpreted by Booker [18] in 1967. Such a phenomenon was first reported to visualize crystalline defects in different metals by Clarke [19] in 1971. It was further utilized for defect analysis in Si by Morin [20] in 1974, who also termed it as electron channeling contrast imaging (ECCI). It enables the generation of a strong crystalline defect contrast which can be used for advanced defect analysis [21-29]. Nowadays, ECCI is widely applied for crystalline defect analysis in metallurgy and semiconductors and ECP is mainly used to align the sample so that channeling conditions can be reached to enable ECCI.

In general, there are two main ways to acquire ECP in backscattering mode: (i) large area channeling pattern (LACP) [30] can be obtained through scanning large areas whereas (ii) selected area channeling pattern (SACP) [31-32] can be acquired through rocking the beam over a small area down to ~ sub-micrometer distances. For single crystalline materials, high quality ECPs can be acquired in both modes and ECCI can be carried out in backscatter geometry. However, both LACP and SACP modes still face great challenges on polycrystalline (especially ultrafine-grained) materials. In such a case, acquiring high quality ECPs remains difficult due to the small grain size. Channeling conditions are hence hard to determine. As a result, ECCI is mostly carried out in forward scatter geometry with the help of EBSD to align the sample to proper channeling conditions. Furthermore, different forward scatter methods, i.e. controlled ECCI [23], accurate ECCI [33], rotational ECCI [34] and open ECCI [35] have been developed to carry out ECCI on polycrystalline materials. A detailed comparison between forward and backward scatter ECCI geometry can be found in reference [23].

Since ECP carries the information about crystal structure and orientation, it can be used to determine lattice parameters, grain orientations, strains, and defect densities [36]. For example, Electron CHanneling ORientation Determination (eCHORD) [37] based on ECP has been developed for the determination of polycrystal grain orientations. However, the application is limited due to complicated and time-consuming measurements and data analyses. Most semiconductor materials and devices are built on top of single crystal wafers with fixed zone axis, e.g. Si(001) or Si(111) substrates. Hence, high quality ECPs can be acquired in backscatter geometry. For instance, a square area formed by 4 equivalent {220} ECBs is always expected in the pattern center for Si(001) wafers. These ECPs have the potential to provide an absolute angular resolution of ~ 0.1° with respect to the optical axis [18]. Since the wafer offcut angle represents the deviation of the zone axis with respect to the surface normal, the ECP can be used to derive the wafer offcut angle as well as the misorientation of the overlaying films.

This study will introduce detailed methods to achieve these goals and presents results obtained in example situations including samples with low and high offcut angles in addition to silicon-on-nothing

(SiON) samples [38]. This work will highlight the potential of the technique as a fast, accurate and cost-effective option to determine the wafer offcut angles and misorientations for research and industrial applications.

2. Materials and tools

To evaluate the potential of the different methods for wafer offcut angle measurements, this study utilizes two types of blanket Si(001) wafers with offcut angles of ~ (0°±1°) and ~ (6°±1°), as illustrated in Fig.1a. The angular tolerance of ±1° is provided by the wafer supplier. To characterize misorientations between different regions, a silicon-on-nothing sample is used. The sample has a plate-shaped void with a size of 150 mm x 150 mm in the center of a 200 mm silicon wafer. Parts of the void and Si bulk regions are shown in Fig. 1b. Prior to measurements, the wafers were cleaved into small coupon pieces of ~ 3 cm x 3 cm to fit into the SEM chamber. On the SiON coupon, both SiON and Si bulk regions are present and used for relative comparisons.

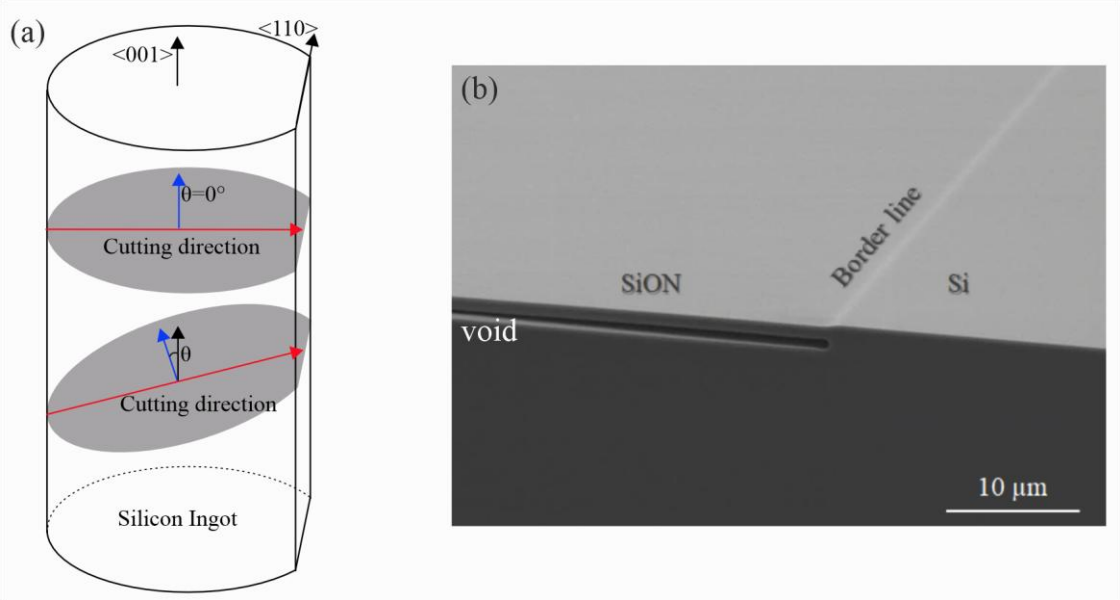

Fig.1 (a) Schematic illustrating wafers with different offcut angles. (b) Tilted cross-section SEM imaging showing the border between silicon-on-nothing (SiON) and Si bulk structures.

The ECP measurement is carried out using an Apreo SEM tool from Thermo Fisher Scientific. A retractable annular solid-state semiconductor detector situated between the pole piece and the sample is inserted, as shown in Fig. 2, to collect the BSE signals. A beam voltage of 20 kV and a beam current of 0.8 nA are used at a working distance (WD) of 5 mm to acquire ECPs with an angular range of ~ 4°. The corresponding beam diameter is ~ 3.9 nm and the beam convergence angle is ~5 mrad. The applied convergent beam angle guarantees the quality of the acquired ECP as explained in reference [21]. The sample stage allows for the sample to be rotated around the z-axis in the [0°, 360°] range. At the applied

WD, the stage tilting range around the x-axis is approximately [-10°, 10°] with the insertion of the BSE annular detector. For both rotation and tilting, the minimum step is 0.1°.

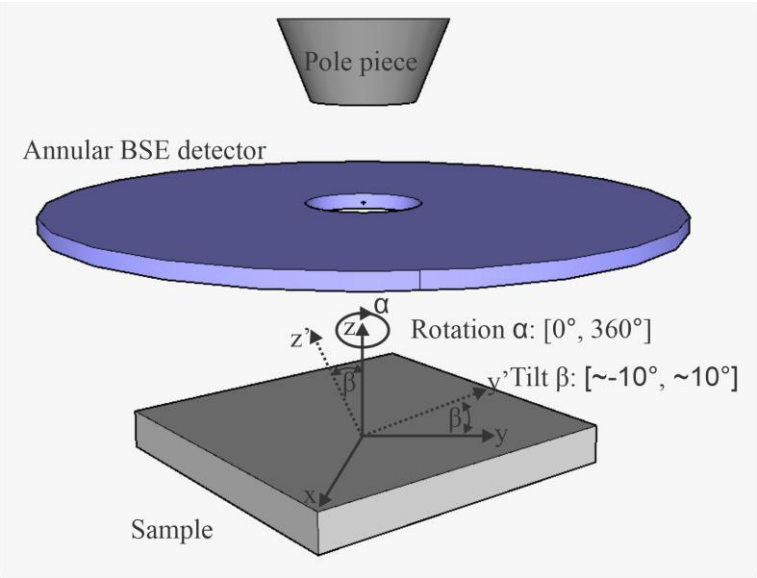

Fig. 2 Schematic illustration of the tool setup with the annular BSE detector inserted. The sample stage can continuously rotate around the z-axis in the range of [0°, 360°] and tilt around x-axis in the range of [-10°, 10°] while the annular BSE detector is present.

Wafer offcut angle measurements using HRXRD are conducted using an X'pert diffractometer from PANalytical B.V. equipped with a PIXcel3D detector. During the measurement, the orientations of the wafer surface and Si (004) planes with respect to the X-ray beam are measured using the in-plane φ-scan and related ω-scans, respectively. The orientation difference between them is used to determine the wafer offcut angle and its direction. Detailed measurement procedures can be found in reference [11].

3. Methodology

An ECP (Fig. 3a) of an on-axis (001) Si wafer is simulated using the EMsoft simulation suite [39]. It covers an angular range of ~ 150 mrad (~ 8.6°). The [001] zone axis, surface normal and electron beam are parallel to each other, and they coincide at the ECP center. Samples without offcut angles (Fig. 3b) exactly correspond to the simulation. The related ECP is indicated by a yellow square in Fig. 3a. For samples with an offcut angle θ (Fig. 3c), which is the angle between the [001] zone axis and surface normal, the corresponding ECP is denoted by a green square in Fig. 3a. The surface normal (red dot) stays at the ECP center whereas the [001] zone axis (blue dot) is shifted away from the surface normal. When tilting the sample, the ECP moves as it is rigidly fixed with the [001] zone axis. If the sample is rotated around the surface normal, the ECP together with the zone axis will rotate around the surface normal in the same way. During sample rotation, the surface normal is identical to the ECP rotation

center. The angular distance between the [001] zone axis and the surface normal, or ECP rotation center, is defined as the wafer offcut angle θ.

The workflow used to determine the wafer offcut angle using ECP is shown in Fig. 4.

1. The wafer/sample is loaded into the SEM chamber.
2. The sample surface normal should be aligned parallel to the primary electron beam. The beam center (usually at/around the image geometrical center) is defined as the position in the image, around which the beam is tilted during the scanning process. This alignment can be done by checking the WD at 3 or 4 different random positions on the sample surface. If the different positions have identical WD, the sample surface normal is parallel with the optical axis. If not, the sample needs to be tilted/rotated to align the surface normal to the optical axis. The exact WD can be determined through proper focusing on the sample surface (e.g. on small particles generated during cleavage or on the sample edges). Tilting can bring the zone axis back into the field of view, only when it is situated in the tilting direction, otherwise a sample rotation is needed.
3. ECP images are acquired in a stage rotation series. In this study, a stage rotation of 330° with a step of 30° is applied.
4. Check if the zone axis is in the field of view or not through comparing with simulated ECP.
5. If the wafer zone axis is present in the field of view of ECP, a coordinate system based on the ECP image can be established. The zone axis positions recorded at different rotation angles are fitted into a circle. If not, go to step 7.
6. The center of the fitted circle is defined as the ECP rotation center or beam center, and the radius of the circle is the wafer offcut angle.
7. If the zone axis is not present in the field of view, additional stage tilts need to be applied to bring the zone axis in the field of view through comparing with the simulated ECP.
8. At least two tilted ECP images with the zone axis in the field of view should be acquired. The initial position of the zone axis without tilt can be determined from ECP images in the tilting series.
9. The beam center can be determined by fitting a feature from the non-tilted ECP images from the rotation series. The angular distance between the beam center and the initial zone axis is the wafer offcut angle.

The above workflow is carried out manually in this study. It is worth noting that the workflow can be automated using programming.

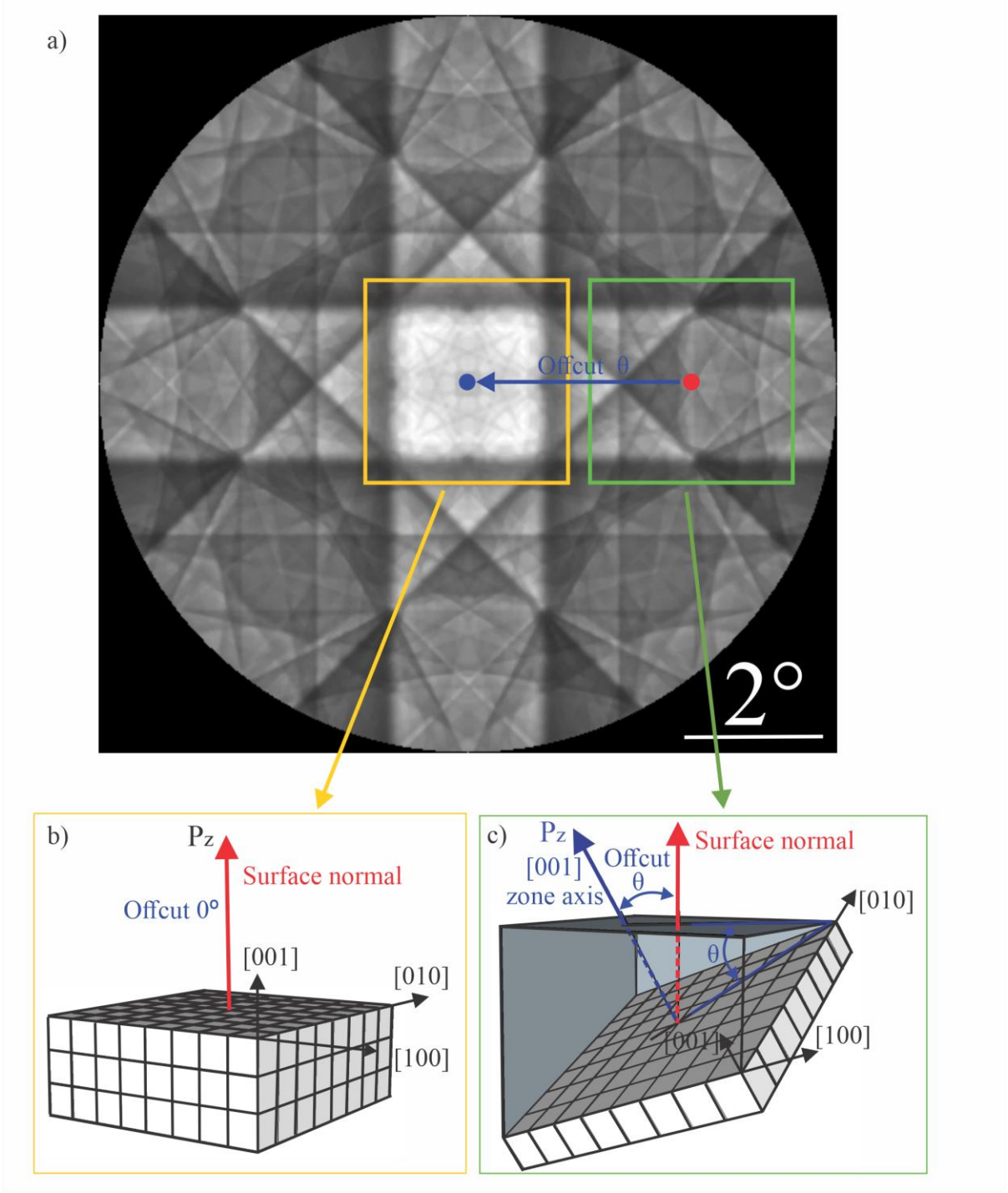

Fig. 3 Schematic illustration showing the principle of determining the wafer offcut angle using ECP. (a) simulated ECP on a Si(001) wafer at 20 keV and 0.8 nA. For samples without offcut (b), the ECP is marked by the yellow square in Fig. 3a. The surface normal is identical to the zone axis [001] at the ECP center. For samples with offcut (c), the ECP may correspond to the area marked by the green square in Fig. 3a. The surface normal (red spot in Fig. 3a) stays at the observed ECP center whereas the [001] zone axis (blue spot in Fig. 3a) is shifted away from the surface normal. The angular distance between the red and blue spots is the wafer offcut angle θ. In practice, the surface normal is unknown, and a rotation is required to determine its position.

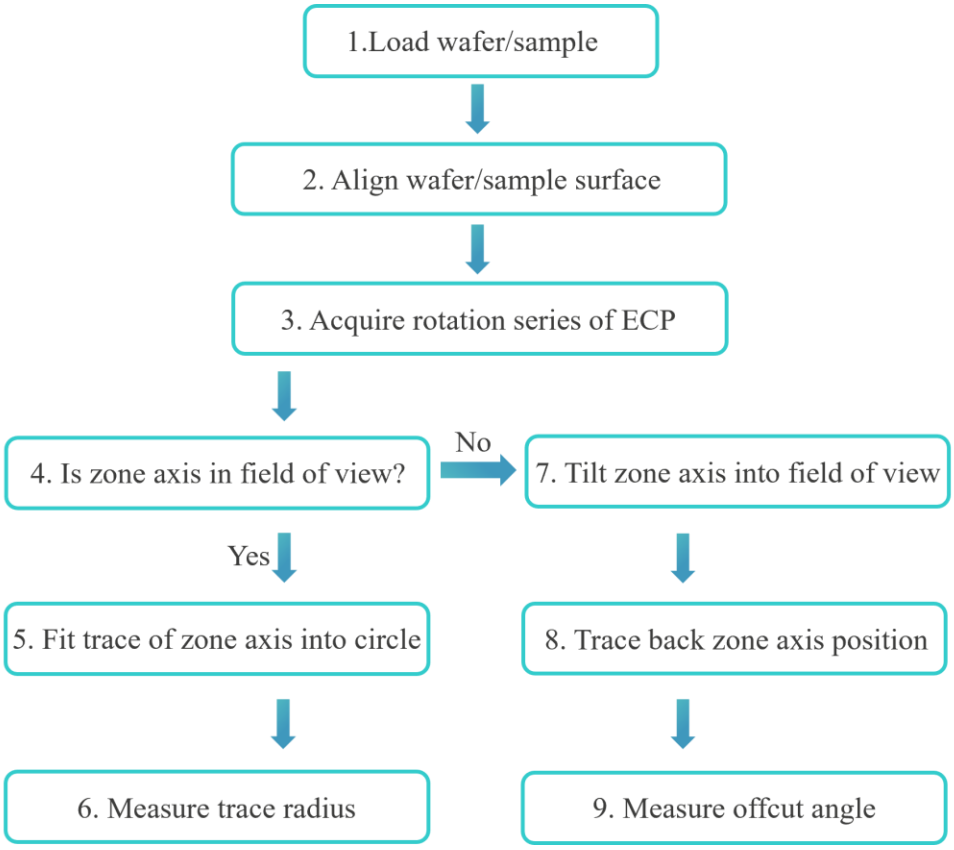

Fig.4 Workflow to determine the wafer offcut angle using ECP.

For the determination of the misorientation between the epi-layer and the substrate, the above workflow is not needed. The misorientation is described by a rotation and/or shift of the ECP, since the ECP is bonded to the specific wafer orientation. When the zone axis is tilted away with an angle, it leads to a related angular shift to the ECP following the tilting direction. Even if the zone axis stays the same, the crystalline orientation can still change by rotation around the zone axis, thus leading to a rotated ECP. Since the rotation can be decomposed into shifts in two different directions, the misorientation can be quantitively measured by the angular ECB shifts along two arbitrary orthogonal directions. The misorientation does not depend on the establishment of the coordinate system but can have different values or expressions in different coordinate systems. It can easily be measured at the boundary between different regions after setting up a coordinate system, as demonstrated in the following paragraphs.

4. Results

4.1 Determination of wafer offcut angles

4.1.1 Determination of low wafer offcut angles

The Si wafers with different offcut angles are first cleaved into small pieces. Afterwards, the workflow described in the previous section was applied on two coupons. The measurements performed on the low offcut angle coupon are shown as follows. After loading and alignment, a series of ECP images at rotation steps of 30° with otherwise the same tool settings were taken and are shown in Fig. 5. As can be seen, during sample rotation, the complete ECP pattern rotates rigidly around the rotation center.

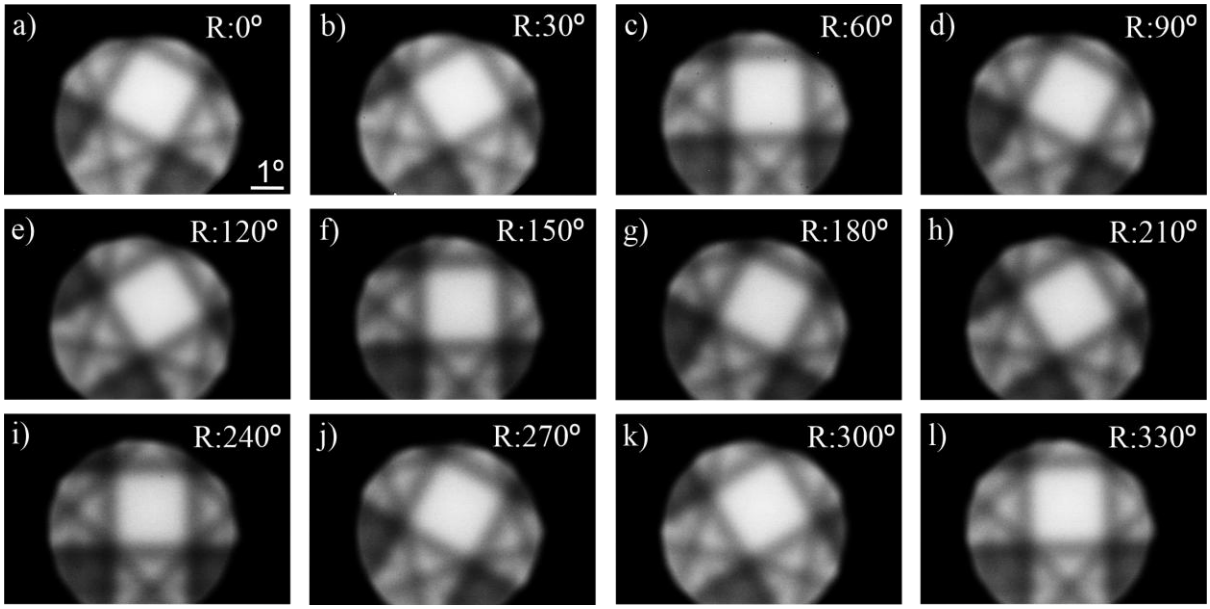

Fig. 5 ECP images acquired from a rotation series. The rotation angles are marked in the image. The rotation step is 30°.

Fig. 6 illustrates how an angular coordinate system was set up and the wafer offcut angle was determined through tracking the positional changes of the [001] zone axis upon sample rotation. The coordinate center is defined at the top left corner and angular axes X and Y follow the horizontal and vertical directions of the image, respectively. The {220}- and {400}- ECBs, indicated on the example ECP image (Fig. 6a) by the broken lines, were used for the angle calibration. These bands form different squares with the [001] zone axis located at the center. As the sample rotates, the angular position of the [001] zone axis forms a circle upon completing the rotation series. The angular positions of the [001] zone axis (black dots) are used to fit a circle (blue) as shown in Fig. 6b. The circle's center indicates the beam center (red dot) and its radius represents the wafer offcut angle. Furthermore, the angular distance between the image's geometrical center (magenta star) and the beam center indicates the beam offset, which is defined as the angle between beam center and image center.

Using the procedure described above, the wafer offcut angle is determined as 0.05° for the Si sample with a low offcut angle, which matches the XRD measurement (0.02°). The beam offset is determined as 0.33° in this case, which means that the beam center deviates slightly from the image center.

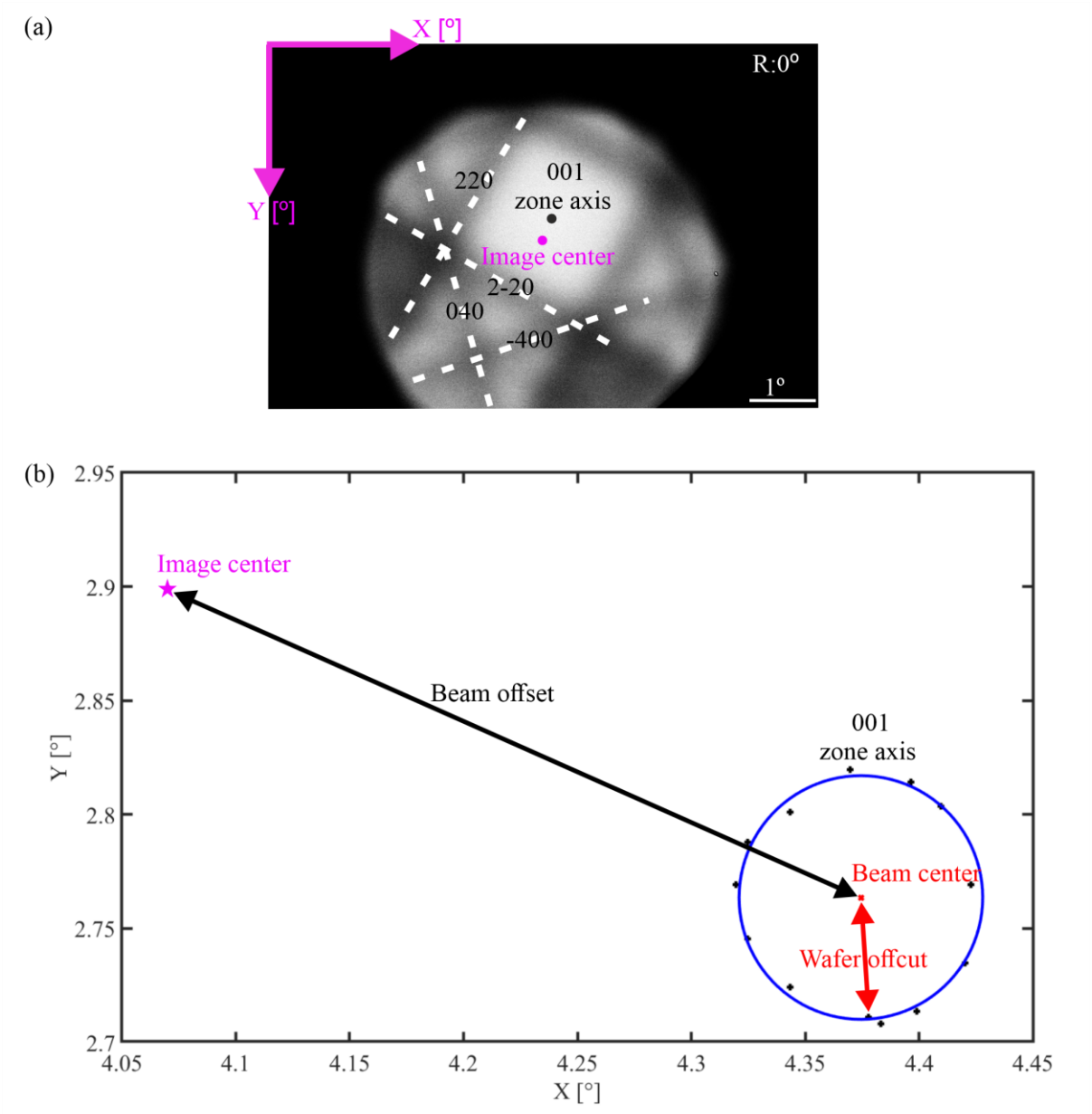

Fig. 6 Establishment of coordinate system based on ECP (a). The [001] zone axis and image center are marked. Some typical ECPs are indexed and marked with broken white lines for better illustration. (b) The trace of the [001] zone axis from a rotation series is plotted to determine the wafer offcut angle. The beam offset is defined as the angle between beam center and image center.

4.1.2 Determination of high wafer offcut angles

Fig. 5 shows clearly that the [001] zone axis is present in the field of view for wafers with low offcut angles. In case of wafers with higher offcut angles (> ~ 3° for the current settings in Apreo SEM system) where the zone axis is not present in the field of view, the rotation series can still be applied to determine the beam center. Furthermore, additional positionings (e.g. tilting/rotation) are needed to localize the position of the zone axis. The procedure is demonstrated in the following paragraph using another high offcut angle coupon.

Fig. 7a-7l shows the ECP from a Si(001) wafer with a high offcut angle. Though the [001] zone axis is not present, parts of the Si {220}- and {400}- bands are observed and one of their crosspoints at high angles (marked as F) can be used to find the position of the beam center during the rotation series. Following the procedure described above, the ECP was acquired during a rotation series with a step of 30°. After the coordinate system has been established in the same way as shown in the previous case, the trace of F (marked as a white spot in Fig. 7a) is utilized to determine the beam center as plotted in Fig. 7q. Afterwards, the sample tilt is needed to bring the [001] zone axis into the field of view. To determine the position of the [001] zone axis accurately, a series of four tilting angles (5.6°, 6.0°, 6.5°, and 7.0°) are used. ECPs from the tilting series are shown in Fig. 7m-7p for demonstration. The positions of the [001] zone axis at different tilting angles are marked as T1, T2, T3 and T4 (Fig. 7), respectively. Such points are then used to create a tilting trace through a linear extrapolation. The initial [001] zone axis is located on this line and is determined by setting the tilting angle as 0°. The wafer offcut angle is then measured as 6.07°, whereas it is 6.04° using the HRXRD measurement. Similarly, a small beam offset of 0.34° is observed in this case.

Table 1 summarizes the measurement of different samples using ECP and XRD. The angular difference between the two methods is 0.03° for both samples. Note that both methods are in good agreement when taking the measurement errors into consideration. A detailed analysis on the measurement errors is presented in the discussion part.

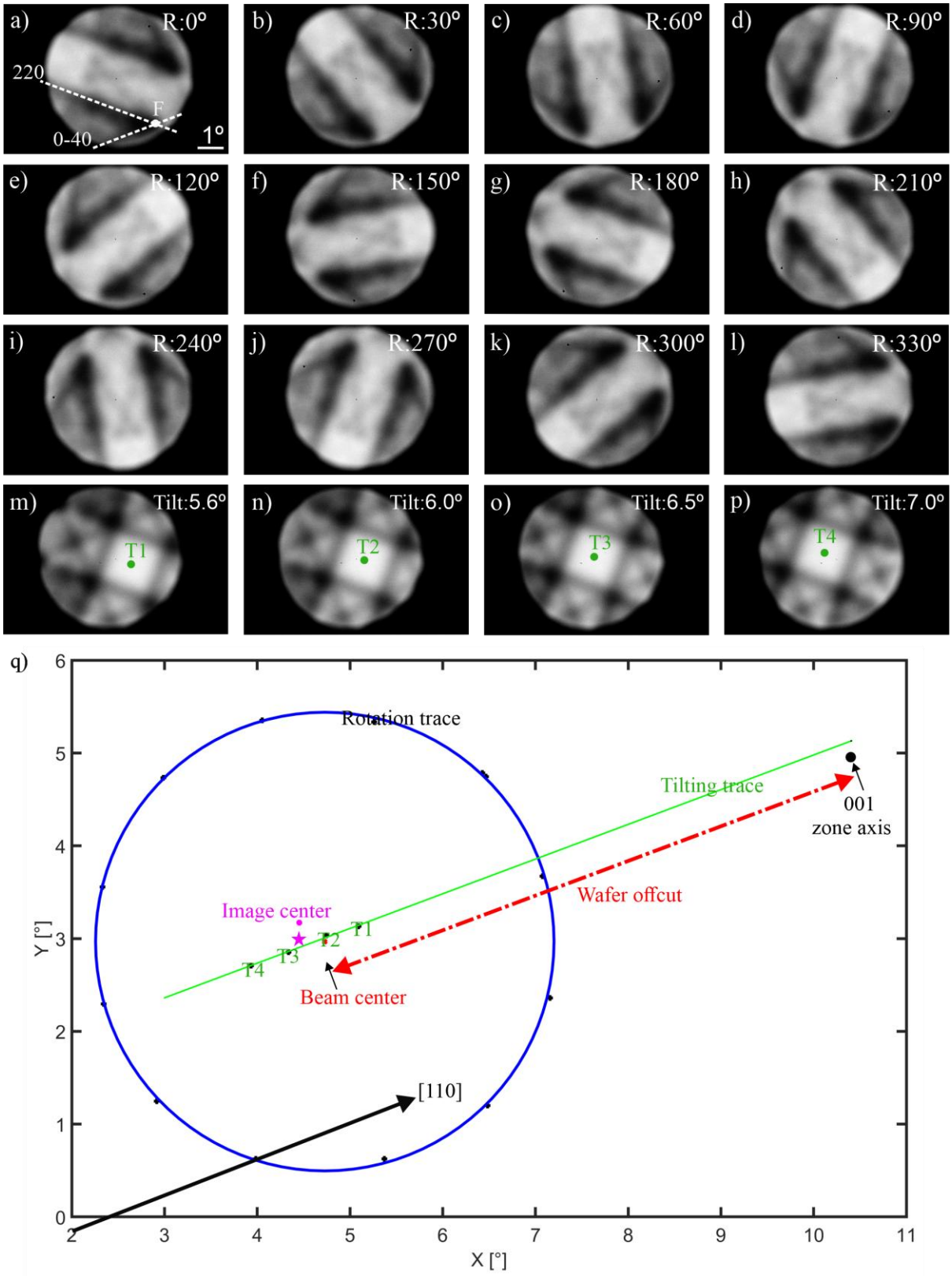

Fig. 7 (a)-(l) ECP images of a Si(001) wafer with a high offcut angle acquired from a rotation series. (m)-(p) ECP images of the same wafer acquired from a tilting series with [001] zone axis in the field of view. The rotation or tilting angles are marked in the image, respectively. The rotation step is 30°. The trace of feature F from the rotation series is plotted to determine the position of the beam center whereas

the trace of [001] zone axis from the tilting series is used to trace back the initial position of the [001] zone axis. The wafer offcut angle is determined as the angular distance between the [001] zone axis and the beam center.

Table 1 Summary of measured Si wafer offcut angles and errors.

Samples	Wafer specifications	Offcut angle using ECP	Offcut angle using XRD
Low offcut	0º ± 1º	0.05º ± 0.05º	0.02º ± 0.01º
High offcut	6º ± 1º	6.07º ± 0.05°	6.04º ± 0.01º

4.2 Determination of misorientation

In theory, any arbitrary coordinate system can be set up for a misorientation measurement. For simplicity, an orthogonal coordinate system based on [100] and [010] crystalline directions can be chosen. The measurement is demonstrated using the SiON sample. During fabrication, the SiON region could suffer from an orientation change whereas the Si bulk still follows the orientation of the pristine Si substrate. As a result, the misorientation between SiON and Si bulk regions is identical to that between the SiON and Si substrate. Such a misorientation can be described by angular shifts along the [100] and [010] directions. They can be characterized through analyzing the (0-40)/(400) ECB shifts between the SiON and Si bulk regions, respectively. The ECB position is defined as the position with the lowest intensity. The band shifts can be identified by measuring the angular position difference between two regions. An example of such measurements is shown in Fig. 8.

A cartesian coordinate system was established by arbitrarily choosing a point of origin (red spot marked in Fig. 8a). Because the border line (broken white line marked in Fig. 8a) indicates the [1-10] direction, [100] and [0-10] directions can be determined accordingly to denote x and y axes, respectively. To determine the angular shift along the [100] direction, two intensity profiles have been plotted at both the SiON (line 1) and Si bulk (line2) regions using Image J, respectively. Both profiles start from the [0-10] axis and run through the (400) band. The band positions are determined by fitting the profiles using the Extreme function defined in Origin 2017. Similarly, the angular shift along the [010] direction is determined through the profiles along line 3 and line 4. The misorientations are measured as 0.07º±0.03º and 0.05º±0.03º along the [100] and [010] directions, respectively. There are potential deviations with regard to the [100] and [010] crystalline orientations during establishment of the coordinate system. However, such deviations will not influence the absolute value of the misorientation. It should be noted that since the BSE information depth at 20 kV is ~ 500 nm [40], the BSE signal forming the ECP is mainly originating from the 1-µm-thick Si membrane and the BSE signal from the wafer underneath mainly contributes to the image background.

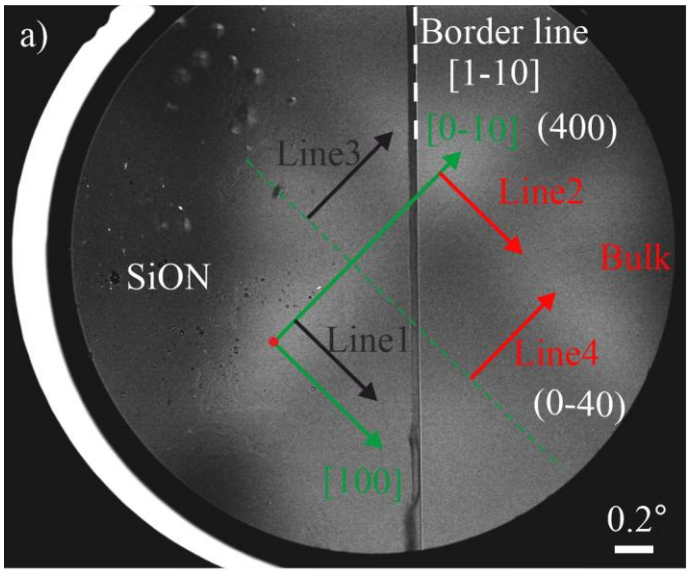
a)
Border line
[1-10]
[0-10]
(400)
Line3
Line2
Bulk
SiON
Line1
Line4
(0-40)
[100]
0.2°

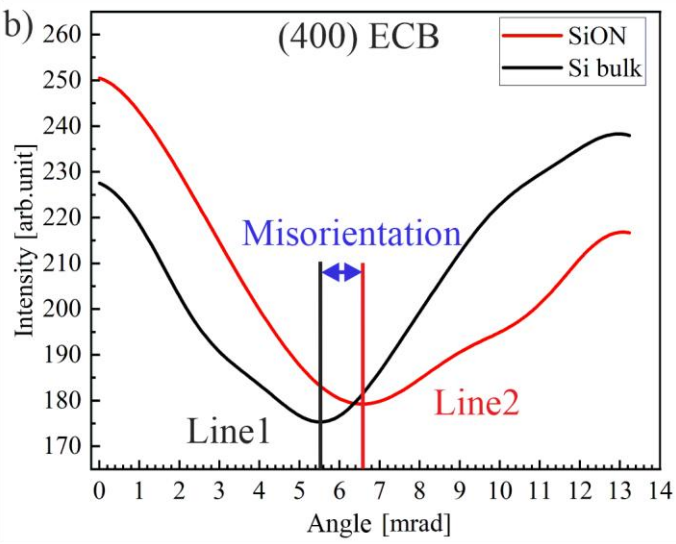
b)
(400) ECB
SiON
Si bulk
Intensity [arb.unit]
Misorientation
Line2
Line1
Angle [mrad]

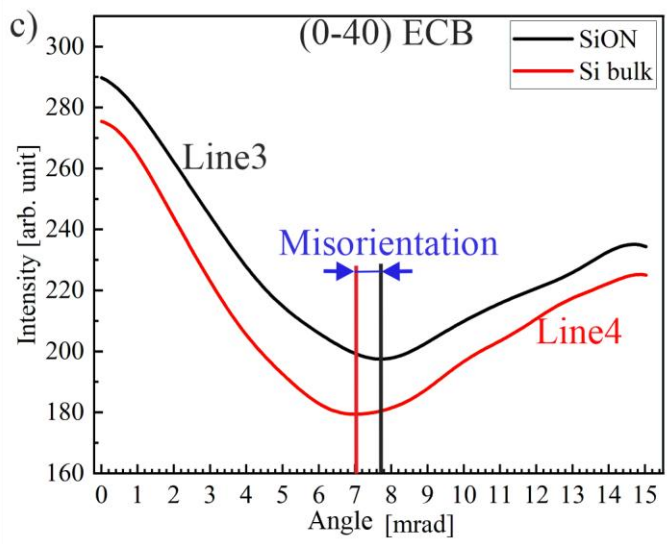
c)
(0-40) ECB
SiON
Si bulk
Intensity [arb. unit]
Line3
Misorientation
Line4
Angle [mrad]

Fig. 8 ECP of SiON sample (a) at the boundary between SiON and Si bulk regions. The border line between SiON and bulk regions is marked by the white broken line and indicates the {1-10} crystalline planes. A coordinate system is established to indicate where the line-scans of line 1 and line 2 begin. The starting positions of line 3 and line 4 are set at the green broken dotted line (parallel to [100] direction) to simplify the process. (b) Intensity profiles of (400) ECB along line 1 and line 2 as marked in SiON and bulk regions, respectively. (c) Intensity profiles of (0-40) ECB acquired in the same way from SiON and bulk regions, respectively. The misorientations can be described by the angular band shift marked on intensity profiles.

5. Discussion

The method allows for a fast and accurate determination of the wafer offcut angle and misorientation. The angular accuracy is determined by several factors. The dominating error ($Error_{align}$) stems from the imperfect sample alignment. When the sample surface normal is aligned parallel to the optical axis of the SEM system, the zone axis rotates around the surface normal (optical axis) upon stage rotation. Otherwise, both the zone axis and surface normal will rotate around the optical axis. As a result, during characterization the misaligned angle between the surface normal and the optical axis will add to the uncertainty. Before the measurement the surface can be properly aligned by tuning the WDs at 3 or 4 random positions (not on one line). During tuning, the distance between different positions should be large enough to detect a WD difference. The identical WD indicates an ideal alignment. Otherwise, tilting and/or rotation of the stage can be applied to keep the WD difference in an acceptable range. This range can be adjusted to some degree according to the accuracy requirement. It is worth noting that achieving high accuracy can be time-consuming, and it is limited by the SEM stage. The stage rotation error is significantly minimized through the circle fit of different rotation steps. In this study, the WD difference was recommended to be tuned within a range of 0.01 mm for distances no shorter than 20 mm, which corresponds to a surface misalignment of ~ 0.029° and a total error within 0.05°. A second important error can be generated during the measurement on ECP images ($Error_{mea}$). It further suffers from the ECP distortion due to uncorrected lens aberrations, especially at image edges. To minimize $Error_{mea}$, the measurements should be done at least 3 times to obtain a good average, preferentially from image center regions. With the applied tool settings in this work, 1 pixel from the experimental ECP image denotes theoretically 0.007º. This pixel resolution is however restricted by the beam convergent angle and image size. In practice, an $Error_{mea}$ value down to 4 pixels (~ 0.028º) can be reached. A third error is due to the electron beam instability ($Error_{insta}$). The beam center shifts slightly every time when the e-beam is switched on. For the Apreo SEM system, the beam varies within a range of ~ 0.025º after 10 measurements. Because the above-mentioned errors are independent of each other, they can be added together using the root sum squared method shown in equation (1).

$$Error_{total} = \sqrt{Error_{align}^2 + Error_{mea}^2 + Error_{insta}^2} \quad (1)$$

According to equation (1), the total error turns out to be 0.0474º, and can be approximated to 0.05º, which is the angular accuracy of the ECP method. Although the accuracy is lower than that of HRXRD (0.01º), it is better than that of EBSD (0.1º). It can satisfy most technical needs of scientific research and industrial production in the nanoelectronics domain.

The results of wafer offcut angle measurements using ECP and XRD are summarized in Table 1. The absolute value from ECP is 0.03° higher than that from XRD for both samples. However, if the errors of ECP (0.05°) and XRD (0.01°) are taken into consideration, the discrepancy lies in an acceptable range. This angular difference of 0.03° seems to be mainly caused by the sample misalignment (0.029°). Although the alignment can be corrected by checking the WD at 3 or 4 random positions, the tuning accuracy is limited by the minimum tilting step of the SEM tool stage (0.1°). When the results from ECP measurements are offset by the misalignment value, both methods match quite well and provide reliable and accurate results. The misalignment error can be significantly minimized by introducing accurate goniometers to the SEM system. Moreover, the angular accuracy can further be improved by optimizing the SEM optical systems.

The key procedure to determine the wafer offcut angle lies in the ECP rotation. A feature of interest should be trackable during rotation to find the beam center. Note that there can be situations that the feature of interest can run out of the field of view during rotation, thus rendering the described procedures unsuccessful. To avoid such situations, a proper feature of interest and a larger field of view of ECP should be used. Ideally the feature of interest should be around the image center and easy to recognize/measure. At the same time, a higher beam voltage (maximum 30 kV in used SEM system) and shorter WD (depending on the spacious position of the retractable detector in the SEM system) should be applied to achieve a larger field of view. Furthermore, the hardware of the most advanced generation SEM systems allows for SACP, which can provide a significantly larger field of view compared to LACP. The SACP makes it easier to generalize the method to other crystalline materials. When the method is applied to hexagonal patterns, e.g. GaN (0001) or Si (111) or sapphire wafers, the rotation step should be carefully chosen to trace the feature due to the 6-fold symmetry. For the strongly insulated sapphire substrate, the influence of charging on the acquisition of ECP can be ignored in the LACP mode, as the charges are distributed in the range of square millimeters for the applied settings in this study. Compared to LACP, the scanned area of SACP can be down to ~100 square micrometers. As a result, a short dwell time and a relatively low beam current should be applied to minimize the influence of charging in SACP mode.

In terms of misorientation between different regions, the angular accuracy is determined by the working distance and beam energy. With increasing working distance, the angular resolution can be increased. However, it is at the expense of a small field of view of the ECP. A lower beam energy can provide a

higher angular resolution, thus sacrificing the field of view of the ECP. Because the accuracy of the misorientation measurement is affected neither by the alignment error ($Error_{align}$) nor by the beam instability ($Error_{insta}$), only the measurement error ($Error_{mea}$) is considered (~ 0.03º) in this case. The error can be reduced further by correcting the lens aberrations.

The misorientation measurement in this study is based on a laboratory SEM system (Apreo SEM tool from Thermo Fisher Scientific). It cannot be used to measure full wafers in the cleanroom. To monitor the orientation change of an epitaxial layer during the semiconductor device fabrication, an inline SEM system equipped with two features is needed: (1) it has the ECP measurement option, and (2) its gun tilting can be accurately controlled and calibrated. For the moment there is no such commercial product on the market yet. Therefore, X-ray diffraction is right now the standard method for such measurements in the semiconductor industry.

Furthermore, the direction of the wafer offcut can be determined from ECP. An example is presented here using the Si(001) high offcut wafer, for which the wafer offcut angle direction can be determined through fitting the tilting series as denoted by the green line in Fig. 7d. The [110] direction can be directly determined from the ECP acquired. The angle between them defines where the wafer offcut is with respect to the [110] direction on the wafer. In this case, the angle is ~ 0.11º, which agrees with the XRD measurement.

The wafer offcut angle can be measured within one hour using the ECP method. It requires 12-16 ECP images which can be acquired in ~ 20 minutes. The post-ECP analysis can be done within ~ 30 minutes once the routine procedures are properly setup. The measurement time can further be decreased when automation is applied for ECP imaging and data analysis. Compared to the HRXRD and EBSD methods which take several hours to complete the measurement and data analysis, the ECP method is much faster and more efficient. Regarding the misorientation characterization, it can be done within 30 minutes, with an accuracy down to 0.03º.

6. Conclusions

We demonstrate a novel approach based on electron channel patterns to determine the wafer offcut angle and the misorientation between different crystalline regions of a given sample. Using this method, the wafer offcut angle can be characterized with an angular accuracy of ~ 0.05º. In terms of misorientation, the angular accuracy can be as low as ~ 0.03º. As a fast, accurate, and easy-to-use technique, it has wide applications, especially in the semiconductor field. This approach can easily be generalized to Si substrates with various zone axes and other substrates, e.g. Si(111) or, sapphire substrates.

Acknowledgements

The authors acknowledge the imec core CMOS program members for their support.

Reference

[1] W.I. Wang, Molecular beam epitaxial growth and material properties of GaAs and AlGaAs on Si (100), Appl. Phys. Lett. 44 (1984) 1149–1151. https://doi.org/10.1063/1.94673

[2] P.N. Uppal, H. Kroemer, Molecular beam epitaxial growth of GaAs on Si(211), J. Appl. Phys. 58 (1985) 2195–2203. https://doi.org/10.1063/1.335987

[3] S. Chen, W. Li, J. Wu, et al., Electrically pumped continuous-wave III–V quantum dot lasers on silicon, Nat. Photon. 10 (2016) 307–311. https://doi.org/10.1038/nphoton.2016.21

[4] M. Sarzynski, M. Leszczynski, M. Krysko, J.Z. Domagala, R. Czernecki, T. Suski, Influence of GaN substrate off-cut on properties of InGaN and AlGaN layers. Cryst. Res. Technol. 47 (2012) 321-328. https://doi.org/10.1002/crat.201100491

[5] L. Huang, F. Liu, J. Zhu, R. Kamaladasa, E.A. Preble, T. Paskova, K. Evans, L. Porter, Y.N. Picard, R.F. Davis, Microstructure of epitaxial GaN films grown on chemomechanically polished GaN(0001) substrates, J. Cryst. Growth 347 (2012) 88-94. https://doi.org/10.1016/j.jcrysgro.2012.03.002.

[6] K. Zhou, H. Ren, J. Liu, M. Ikeda, Y. Ma, S. Gao, C. Tang, H. Yang, Surface morphology and optical properties of InGaN/GaN multiple quantum wells grown on freestanding GaN (0001) substrates, Superlattices Microstruct 100 (2016) 968-972. https://doi.org/10.1016/j.spmi.2016.10.067.

[7] R. Schewski, M. Baldini, K. Irmscher, A. Fiedler, T. Markurt, B. Neuschulz, T. Remmele, T. Schulz, G. Wagner, Z. Galazka, M. Albrecht, Evolution of planar defects during homoepitaxial growth of β-Ga2O3 layers on (100) substrates—A quantitative model, J. Appl. Phys. 120 (2016) 225308, https://doi.org/10.1063/1.4971957.

[8] Y. Shi, B. Groven, J. Serron, X. Wu, A. Nalin Mehta, A. Minj, S. Sergeant, H. Han, I. Asselberghs, D. Lin, S. Brems, C. Huyghebaert, P. Morin, I. Radu, M. Caymax, Engineering Wafer-Scale Epitaxial Two-Dimensional Materials through Sapphire Template Screening for Advanced High-Performance Nanoelectronics, ACS Nano. 15 (2021) 9482-9494. https://doi.org/10.1021/acsnano.0c07761.

[9] J.E. Ayers, S.K. Ghandhi, L.J. Schowalter, Crystallographic tilting of heteroepitaxial layers, J. of Cryst. Growth 113 (1991) 430-440. https://doi.org/10.1016/0022-0248(91)90077-I.

[10] P. Maigné, A.P. Roth, C. Desruisseaux, D. Coulas, 1992. Epitaxial tilt of partially relaxed InGaAs layers grown on (100) GaAs substrates, Can. J. Phys. **70** (1992) 838-842. https://doi.org/10.1139/p92-133

[11] M.A.G. Halliwell, S.J. Chua, Determining substrate orientation using a high-resolution diffractometer, J. Cryst. Growth 192 (1998) 456-461. https://doi.org/10.1016/S0022-0248(98)00474-6.

[12] L.D. Doucette, M. Pereira da Cunha, R. J. Lad, Precise orientation of single crystals by a simple x-ray diffraction rocking curve method, Rev. Sci. Instrum. 76 (2005) 036106. https://doi.org/10.1063/1.1867392.

[13] F.J. Humphreys, Y. Huang, I. Brough, C. Harris, Electron backscatter diffraction of grain and subgrain structures - resolution considerations, J. Microsc. 195 (1999) 212-216. https://doi.org/10.1046/j.1365-2818.1999.00579.x.

[14] A. J. Wilkinson, G. Meaden, and D.J. Dingley, High resolution mapping of strains and rotations using electron backscatter diffraction, Mater. Sci, Tech. Ser. 22 (2006) 1271-1278. https://doi.org/10.1179/174328406X130966

[15] F.J. Humphreys, Review Grain and subgrain characterisation by electron backscatter diffraction, J. Mater. Sci. 36 (2001) 3833–3854. https://doi.org/10.1023/A:1017973432592

[16] P.B. Hirsch, A. Howie, and M.J. Whelan, On the production of X-rays in thin metal foils, Philos. Mag. 7 (1962) 2095–2100. https://doi.org/10.1080/14786436208214478

[17] D.G. Coates, Kikuchi-like reflection patterns obtained with the scanning electron microscope, Philos. Mag. 16 (1967) 1179–1184. https://doi.org/10.1080/14786436708229968

[18] G.R. Booker, A.M.B. Shaw, M.J. Whelan, P.B. Hirsch, Some comments on the interpretation of the 'kikuchi-like reflection patterns' observed by scanning electron microscopy, Philos. Mag. 16 (1967) 1185–1191. http://doi.org/10.1080/14786436708229969

[19] D.R. Clarke, Observation of crystal defects using the scanning electron microscope, Philos. Mag. 24 (1971) 973-979. https://doi.org/10.1080/14786437108217061

[20] P. Morin, M. Pitaval, D. Besnard, and G. Fontaine, Electron–channelling imaging in scanning electron microscopy, Philos. Mag. A 40 (1979) 511–524. https://doi.org/10.1080/01418617908234856

[21] A.J. Wilkinson, G.R. Anstis, J.T. Czernuszka, N.J. Long, P.B. Hirsch, Electron channelling contrast imaging of interfacial defects in strained silicon-germanium layers on silicon, Philos. Mag. A 68 (1993) 59-80. https://doi.org/10.1080/01418619308219357.

[22] B.A. Simkin, M.A. Crimp, An experimentally convenient configuration for electron channeling contrast imaging, Ultramicroscopy 77 (1999) 65-75. https://doi.org/10.1016/S0304-3991(99)00009-1.

[23] I. Gutierrez-Urrutia, S. Zaefferer, D. Raabe. Electron channeling contrast imaging of twins and dislocations in twinning-induced plasticity steels under controlled diffraction conditions in a scanning electron microscope, Scr. Mater. 61 (2009) 737-740. https://doi: 10.1016/j.scriptamat.2009.06.018

[24] S. Zaefferer, N.N. Elhami, Theory and application of electron channelling contrast imaging under controlled diffraction conditions, Acta Mater. 75 (2014) 20-50. https://doi.org/10.1016/j.actamat.2014.04.018.

[25] H. Kriaa, A. Guitton, N. Maloufi, Fundamental and experimental aspects of diffraction for characterizing dislocations by electron channeling contrast imaging in scanning electron microscope, Sci Rep 7(2017) 9742. https://doi.org/10.1038/s41598-017-09756-3

[26] H. Han, T. Hantschel, A. Schulze, L. Strakos, T. Vystavel, R. Loo, B. Kunert, R. Langer, W. Vandervorst, M. Caymax, Enhancing the defect contrast in ECCI through angular filtering of BSEs, Ultramicroscopy 210 (2020) 112922. https://doi: 10.1016/j.ultramic.2019.112922.

[27] H. Han, T. Hantschel, L. Strakos, T. Vystavel, M. Baryshnikova, Y. Mols, B. Kunert, R. Langer, W. Vandervorst, M. Caymax, Application of electron channeling contrast imaging to 3D semiconductor structures through proper detector configurations, Ultramicroscopy 210 (2020) 112928. https://doi: 10.1016/j.ultramic.2019.112928.

[28] H. Yan, E. Postelnicu, T. Nguyen, S. Corujeira Gallo, A. Stacey, K. Mukherjee; Multi-microscopy characterization of threading dislocations in CVD-grown diamond films, Appl. Phys. Lett. 124 (2024) 102108. https://doi.org/10.1063/5.0186842

[29] A. Mandal, B. Beausir, J. Guyon, V. Taupin, A. Guitton, Estimation of Dislocation Densities With Nondestructive Scanning Electron Microscope Techniques: Application to Gallium Nitride, Microsc. Microanaly., 31 (2025) ozae124, https://doi.org/10.1093/mam/ozae124

[30] L. Reimer, Crystal Structure Analysis by Diffraction. In: Scanning Electron Microscopy. Springer Series in Optical Sciences, vol 45. (1998) Springer, Berlin, Heidelberg. https://doi.org/10.1007/978-3-540-38967-5_9

[31] J. Guyon, H. Mansour, N. Gey, M.A. Crimp, S. Chalal, N. Maloufi, Sub-micron resolution selected area electron channeling patterns, Ultramicroscopy 149 (2015) P34-44, https://doi.org/10.1016/j.ultramic.2014.11.004

[32] R.D. Kerns, S. Balachandran, A.H. Hunter, M.A. Crimp, Ultra-high spatial resolution selected area electron channeling patterns, Ultramicroscopy 210 (2020) 112915. https://doi.org/10.1016/j.ultramic.2019.112915

[33] H. Mansour, J. Guyon, M.A. Crimp, N. Gey, B. Beausir, N. Maloufi, Accurate electron channeling contrast analysis of dislocations in fine grained bulk materials, Scr. Mater. 84–85 (2014) 11-14. https://doi.org/10.1016/j.scriptamat.2014.03.001

[34] G. L'hôte, C. Lafond, P. Steyer et al. Rotational-Electron Channeling Contrast Imaging analysis of dislocation structure in fatigued copper single crystal, Scr. Mater. 162 (2019) 103-107. https://doi: 10.1016/j.scriptamat.2018.10.050

[35] Z. Xu, H. W. Ånes, S. Gorelick, X. Fang, P. Miller, OpenECCI - A Streamlined Open-Source Workflow for Electron Channelling Contrast Imaging of Crystal Defects, BIO Web of Conferences 129 (2024) P07004. https://doi.org/10.1051/bioconf/202412907004

[36] D.C. Joy, D.E. Newbury, D.L. Davidson, Electron channeling patterns in the scanning electron microscope, J. Appl Phys. 53 (1982) 080R81. https://doi.org/10.1063/1.331668.

[37] C. Lafond, T. Douillard, S. Cazottes, P. Steyer, C. Langlois, Electron CHanneling ORientation Determination (eCHORD): An original approach to crystalline orientation mapping, Ultramicroscopy, 186 (2018) 146-149, https://doi.org/10.1016/j.ultramic.2017.12.019.

[38] I. Mizushima, T. Sato, S. Taniguchi, Y. Tsunashima, Empty-space-in-silicon technique for fabricating a silicon-on-nothing structure, Appl. Phys. Lett. 77 (2000) 3290-3292. https://doi.org/10.1063/1.1324987.

[39] S. Singh, M. de Graef, Dictionary Indexing of Electron Channeling Patterns, Microsc. Microanal. 23 (2017) 1-10. https://doi.org/10.1017/S1431927616012769.

[40] J. Pinos, S. Mikmekova, L. Frank, About the information depth of backscattered electron imaging, J. Microscopy 266 (2017) 335-342. https://doi.org/10.1111/jmi.12542.